Environmental Science & Technology

Article

pubs.acs.org/est

Detailed Analysis of Criteria and Particle Emissions from a Very Large Crude Carrier Using a Novel ECA Fuel

Nicholas R. Gysel,[†,‡] William A. Welch,[†,‡] Kent Johnson,[†,‡] Wayne Miller,[†,‡] and David R. Cocker, III*[,†,‡]

[†]Department of Chemical and Environmental Engineering, Bourns College of Engineering, University of California, Riverside, California 92521, United States

[‡]College of Engineering - Center for Environmental Research & Technology, University of California, Riverside 1084 Columbia Avenue, Riverside, California 92507, United States

ABSTRACT: Ocean going vessels (OGVs) operating within emission control areas (ECA) are required to use fuels with ≤0.1 wt % sulfur. Up to now only distillate fuels could meet the sulfur limits. Recently refiners created a novel low-sulfur heavy-fuel oil (LSHFO) meeting the sulfur limits so questions were posed whether nitric oxide (NO_x) and particulate matter (PM) emissions were the same for the two fuels. This project characterized criteria pollutants and undertook a detailed analysis of PM emissions from a very large crude oil carrier (VLCC) using a distillate ECA fuel (MGO) and novel LSHFO. Results showed emission factors of NO_x were ∼5% higher with MGO than LSHFO. $PM_{2.5}$ emission factors were ∼3 times higher with LSHFO than MGO, while both were below values reported by Lloyds, U.S. EPA and CARB. A detailed analysis of PM revealed it was >90% organic carbon (OC) for both fuels. Elemental carbon (EC) and soot measured with an AVL microsoot sensor (MSS) reflected black carbon. PM size distributions showed unimodal peaks for both MGO (20−30 nm) and LSHFO (30−50 nm). Particle number (PN) emissions were 28% and 17% higher with the PPS-M compared to the SMPS for LSHFO and MGO, respectively.

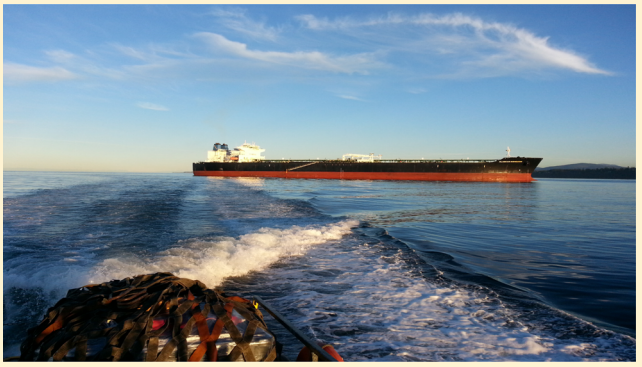

INTRODUCTION

Ocean Going Vessels (OGVs) contribute significantly to port emissions inventories and ∼15% of the global NO_x emissions and 5−8% of global SO_x emissions.[1,2] Furthermore, crude oil carriers comprise ∼29% of the worldwide OGV fleet[3] and approximately 40%[1] of the total ship emissions. Corbett at al. estimates that approximately 70% of ship related emissions occur within 400 km of land or port communities.[2] This has significant implications toward pollution and health effects for communities near large port areas. For instance, Corbett et al.[2,4] estimated that PM emissions from ocean going ships contribute to approximately 60 000 deaths from cardiopulmonary and lung related diseases. Similarly, Pope et al.[5,6] determined that PM emissions contribute to respiratory illnesses and death. OGVs are also a major source of NO_x emissions, which is a precursor to atmospheric ozone (O_3) formation.

While emissions from port on-land activities were being heavily regulated, the percentage of emissions from port activities has increased.[7] MARPOL Annex VI[8] regulates NO_x and SO_x emissions from ships, and in 2008, the International Maritime Organization (IMO) adopted a policy limiting the sulfur content of emissions allowed in Emissions Control Areas (ECA), including: The Baltic Sea, North Sea and English Channel, plus the U.S., most of Canada, the U.S. Virgin Islands and Puerto Rico. From first January 2015, every ship operating within ECA had to use fuels with ≤0.1% sulfur content or existing fuels with the installation of a gas cleaning system that removes sulfur from the exhaust.

Although Annex VI does not directly regulate PM mass emissions, the IMO limited the amount of sulfur content in the fuel and at the time of the regulation, only distillate fuels met the strict sulfur limits. Environmentalists and the shipping community generally supported the regulations for the ECA areas and the expected benefits as sulfur levels were reduced from ∼1.5% before 2010 to 0.10% in 2015. Previous studies have shown[9−16] that PM emissions from engines burning a low-sulfur, distillate fuels were significantly lower when compared with emissions from burning a high-sulfur HFO.

This study provides real world measurements of criteria pollutants and a detailed analysis of the PM and ultrafine particles emitted from a modern, double hull, very large crude oil carrier (VLCC) sailing along the Pacific Coast while burning either a MGO or a low-sulfur HFO (LSHO), both fuels being ECA-compliant.

Received: May 26, 2016
Revised: December 18, 2016
Accepted: January 4, 2017
Published: January 4, 2017

DOI: 10.1021/acs.est.6b02577
Environ. Sci. Technol. 2017, 51, 1868−1875

EXPERIMENTAL METHODS

Vessel and Engine Description. The OGV platform used in this study was a supertanker/VLCC, which is representative of the 2006+ crude oil tankers. The vessel is approximately 941 feet long, has a dead weight (dwt) of 180 000 to 320 000 MT and carries 1.3 million barrel of crude. The vessel is equipped with four main propulsion diesel-electric MAN B&W 6L48/60, 6.3 MW, medium speed engines resulting in a total power of 25.2 MW at 512 rpm and meeting Tier 1 emissions. Additionally, the engines are equipped with variable injection timing (VIT) for lower NO_x emissions. In this study, the emissions from MGO were measured from the starboard side engine and the emissions from the LSHFO were measured from the port side engine.

Fuel Properties. Selected fuel properties for both fuels are summarized in (Table 1). Both fuels have little sulfur, ash and vanadium. Ash and vanadium were not present in the sample analysis. The main differences in the fuel properties are viscosity, pour point and micro carbon residue (MCR). The LSHFO is a novel fuel that is available on the West Coast and some European ports. This fuel provides ship operators with the option of using either a distillate or HFO meeting the required sulfur limits.

Table 1. Fuel Properties for HFO and MGO Fuels

		certificate of analysis (COA)	
fuel	units	LSHFO	MGO
density @ 15 °C	kg/m^3	845.2	850.9
viscosity @ 40 °C	cSt	12.07	3
pour point	°C	18	−24
carbon residue	% m/m	0.03	0.06
sulfur	% m/m	0.009	0.005
ash	% m/m	0	0
vanadium	mg/kg	0	0

Test Cycles/Test Matrix. The emission measurements for this study followed the load points specified in the ISO-8178 E2 cycle were followed as close as possible and the actual load points and percent load are shown in Table 2. The exhaust flow rate was calculated based on the air pump method that uses the engine stroke type, measured RPM, charge air temperature and pressure provided by the engine ECM and assumes a volumetric efficiency of one entering and leaving the cylinder. Prior comparisons conducted in our lab between the carbon balance and air pump methods on OGVs were found to agree within 5% of one another.

Table 2. ISO-8178 and Achieved Load Points

	ISO-8178 E2	mode 1	mode 2	mode 3	mode 4
fuel	ISO load	100	75	50	25
MGO	% load	98%	73%	51%	24%
	MW	6.0	4.5	3.1	1.5
LSHFO	% load	99%	73%	50%	23%
	MW	6.0	4.4	3.0	1.4

[a]MW (Megawatt).

Sampling and Analysis. Measurements of gases and PM were taken according to the ISO-8178-2[17] sampling protocol. The sampling setup utilizing a primary partial flow venturi dilution and secondary ejector type dilution tunnel is shown in Figure 1. Real-time gaseous species NO_x, CO and CO_2 were measured with a HORIBA portable five-gas analyzer (PG-250). PM samples were collected with 2 μm 47 mm diameter Teflo filters (Pall Gelman, Ann Arbor, MI) for off-line gravimetric analysis of total $PM_{2.5}$ mass. The filters net mass was measured with a Mettler Toledo UMX2 microbalance. All weighing procedures were followed per the Code of Federal Regulations (CFR).[18] These filters were conditioned for 24 h in an environmentally controlled room at a relative humidity of 40% and temperature of 25 °C. Teflo filters were subsequently extracted with HPLC grade water and isopropyl alcohol and analyzed for ions using a DX-120 ion chromatograph. $PM_{2.5}$ for subsequent elemental carbon (EC) and organic carbon (OC) analysis were collected on 47 mm diameter, 2500 QAT-UP Tissuquartz (Pall Gelman, Ann Arbor, MI) filters which were preconditioned at 600 °C for 5 h. A 1.5 cm^2 punch from the filter was analyzed with a Sunset Laboratory (Forest Grove, OR) thermal/optical carbon analyzer per the NIOSH 5040 reference method.[19] Sample dilution ratio from the partial flow venturi dilution tunnel (primary diluter) was determined using NO_x and CO_2 measured for raw and dilute conditions. Average primary dilution ratios were 12:1, which were used for the filter samples, the PPS-M sensor, AVL MSS and the PG-250. For the SMPS a ∼ 6:1 ejector diluter (secondary diluter) was used in conjunction with the primary diluter for a combined dilution ratio of ∼72:1. Due to the high dilution and lower limit of the PG-250, the dilution ratio of the secondary dilution tunnel was determined using a flame ionization detector (FID) to measure raw and dilute propane concentrations. The dilution ratios were measured twice at each load condition, before the first and after the third repeat run.

Real-time particulate matter measurements included an AVL model no. 483 Micro Soot Sensor (MSS), which employs a photoacoustic method to measure the solid soot fraction of PM. The Pegasor Particle Sensor (PPS-M) was used to characterize both the solid and condensable fractions of total particulate matter mass and number. The PPS-M sensor uses an "escaping current" method[20] where clean air is ionized and mixed with the sample stream thereby charging the particles. The escaping current from the sample is then measured at a fixed flow rate by a Faraday cup. A default trap voltage of 400 V was used for the PPS-M sensor. The manufacturer recommends a trap voltage of 800 V for most accurate PM mass concentrations and 400 V for particle number correlations. Particle size distributions were measured with a scanning mobility particle spectrometer (SMPS) comprised of a TSI model 3080 classifier, 3081 differential mobility analyzer (DMA) and TSI 3776 condensation particle counter (CPC). In conjunction with the primary diluter- partial flow venturi dilution system, a secondary ejector dilution system was added for additional dilution for the SMPS.

Overall Weighted Emission Factors. The weighted ISO 8178-E2[22] cycle emission factors were calculated per equation:

$$EF_x = \frac{\sum_{i=1}^{i=n} m_i WF_i}{\sum_{i=1}^{i=n} p_i WF_i} \quad (1)$$

where EF_x is the weighted mass emission level in g/kWh of each pollutant and m_i (g/h), WF_i and p_i are the mass emission rate, weighting factor and engine load, respectively, for the ith operating mode. The ISO-8178 E2 test cycle specifies the steady state load points of 25%, 50%, 75%, and 100%. Emissions from the 10% load point were collected to represent

DOI: 10.1021/acs.est.6b02577
Environ. Sci. Technol. 2017, 51, 1868−1875

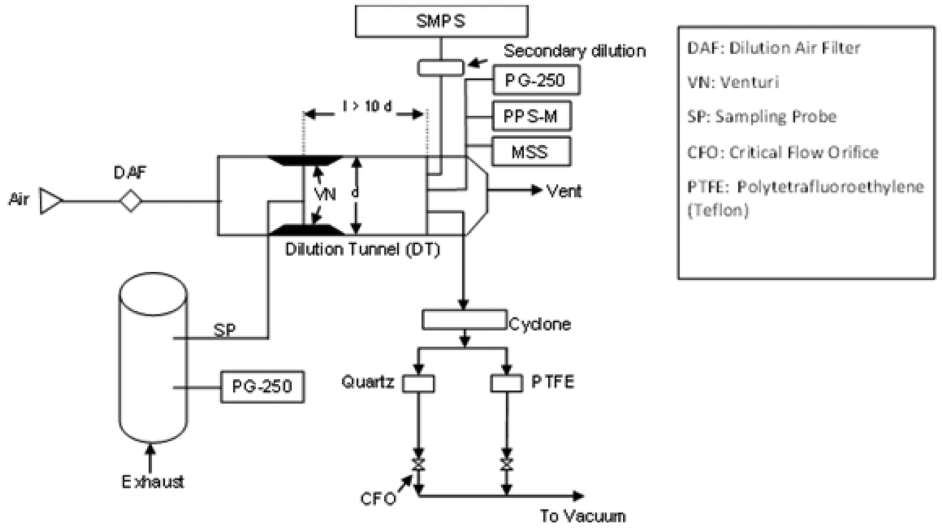

Figure 1. Sampling system flow diagram.

Table 3. Modal and Weighted Gaseous Emission Factors (g/kWh)

	NO_x		CO		CO_2	
load (%)	MGO	LSHFO	MGO	LSHFO	MGO	LSHFO
10[a]	22.8 ± 0.16	15.3 ± 0.50	0.24 ± 0.01	4.7 ± 0.53	1192 ± 10	913 ± 7
25	10.6 ± 0.05	8.9 ± 0.30	0.60 ± 0.30	1.8 ± 0.10	746 ± 7	725 ± 26
50	9.6 ± 0.06	8.6 ± 0.06	0.42 ± 0.05	0.84 ± 0.10	612 ± 4	609 ± 4
75	10.5 ± 0.11	10.9 ± 0.11	0.28 ± 0.03	0.4 ± 0.05	662 ± 2	628 ± 5
100	11.3 ± 0.15	9.8 ± 0.15	0.28 ± 0.01	0.3 ± 0.05	632 ± 10	613 ± 1
wt. avg.	10.7 ± 0.03	10.2 ± 0.03	0.31 ± 0.01	0.5 ± 0.04	652 ± 2	627 ± 5

[a]Not included in Wt. Avg. per ISO-8178 E2 cycle.

Table 4. Modal and Weighted PM Emission Factors (g/kWh)

	PM_{25} Teflon		PM PPS		PM SMPS		PM MSS	
load (%)	MGO	LSHFO	MGO	LSHFO	MGO	LSHFO	MGO	LSHFO
10	1.2 ± 0.12	3.7 ± 0.13	0.7 ± 0.05	2.6 ± 0.06	0.4 ± 0.004	2.6 ± 0.00048	0.1 ± 0.0007	0.2 ± 0.02
25	0.5 ± 0.04	1.7 ± 0.096	0.3 ± 0.01	1.2 ± 0.08	0.2 ± 0.0004	1.2 ± 0.000039	0.05 ± 0.001	0.05 ± 0.004
50	0.2 ± 0.01	0.8 ± 0.03	0.09 ± 0.003	0.5 ± 0.01	0.05 ± 0.0001	0.5 ± 0.0004	0.01 ± 0.0001	0.01 ± 0.00005
75	0.1 ± 0.03	0.6 ± 0.03	0.09 ± 0.01	0.3 ± 0.01	0.05 ± 0.0002	0.3 ± 0.0005	0.01 ± 0.0002	0.01 ± 0.0002
100	0.2 ± 0.04	0.3 ± 0.03	0.08 ± 0.003	0.1 ± 0.01	0.04 ± 0.00004	0.1 ± 0.0001	0.005 ± 0.0003	0.01 ± 0.0002
wt. avg.	0.2 ± 0.02	0.6 ± 0.02	0.08 ± 0.01	0.3 ± 0.005	0.05 ± 0.0002	0.3 ± 0.0003	0.01 ± 0.0001	0.01 ± 0.0004

EC		OC		H_2SO_4*6.5H_2O	
MGO	LSHFO	MGO	LSHFO	MGO	LSHFO
0.1 ± 0.0003	0.2 ± 0.02	1.02 ± 0.014	2.9 ± 0.22	0.007 ± 0.004	0.004 ± 0.0005
0.05 ± 0.002	0.04 ± 0.0004	0.5 ± 0.02	1.3 ± 0.011	0.001 ± 0.0004	0.001 ± 0.00004
0.01 ± 0.0003	0.01 ± 0.0004	0.2 ± 0.004	0.7 ± 0.03	0.001 ± 0.0001	0.002 ± 0.0004
0.01 ± 0.002	0.01 ± 0.0003	0.2 ± 0.03	0.5 ± 0.002	0.001 ± 0.0002	0.002 ± 0.0005
0.004 ± 0.0002	0.01 ± 0.0003	0.1 ± 0.002	0.3 ± 0.005	0.001 ± 0.00004	0.002 ± 0.0001
0.01 ± 0.001	0.01 ± 0.0001	0.2 ± 0.02	0.5 ± 0.002	0.001 ± 0.0002	0.002 ± 0.0003

values expected near idle or low VSR speeds; however, these values were not included in the overall emission factors.

RESULTS AND DISCUSSION

Triplicate measurements were made as a function of engine load point and fuel type for the steady-state ISO-8178 E2 test cycle. Standard deviations denote the deviations from the average of triplicate measurements at each load point. Statistical significance was determined by a two-tailed, paired *t* test with $p \leq 0.05$.

Gaseous Emission Factors. The modal and weighted gaseous emission factors of NO_x, CO and CO_2 for both fuels (g/kWh) are shown in Table 3. Overall, both fuels had the highest observed NO_x emissions at the 10% load point where engines are operating far from their peak efficiencies. NO_x emission factors (g/kWh) for main engine, medium speed OGVs from previous studies are compared against the current in Table 5. NO_x emissions for LSHFO and MGO are well below Lloyds services data,[21] U.S. EPA[10] and CARB,[11] but are similar to the emissions from Celo et al.[23] (8.4 ± 0.03 and 10.7 ± 0.04 g/kWh) for IFO60 and MDO. Slight differences were

DOI: 10.1021/acs.est.6b02577
Environ. Sci. Technol. 2017, 51, 1868−1875

Table 5. Comparison of Main Engine Medium Speed Emission Factors with Literature

main engines (MSD)	fuel	sulfur (%)	NO_x	CO	PM	SO_2
			g/kWh			
measured (weighted)	MGO	0.005	10.7 ± 0.03	0.31 ± 0.01	0.2 ± 0.02	
	LSHFO	0.009	10.2 ± 0.03	0.5 ± 0.04	0.62 ± 0.02	
Lloyds Services data	HFO		13.7	1.59	1.25	
U.S. EPA	MGO	0.5	13.2	0.47	0.29	1.98
	MGO	0.1	13.2	0.31	0.17	0.4
CARB	MGO	0.1	13.2	1.1	0.25	0.4
	MGO	0.1	13.2	1.1	0.38	2.08
	HFO		14.0	1.1	1.5	11.5
Celo et al.	IFO60	1.2	8.4 ± 0.03	1.31 ± 0.02	0.37 ± 0.01	4.7 ± 0.01
	MDO	0.1	10.7 ± 0.04	1.22 ± 0.02	0.30 ± 0.03	0.47 ± 0.1
[a]Winnes et al. (35% load)	MDO	0.5	7.8		0.0088 ± 0.003	
	HFO	0.1	7.2		0.65 ± 0.11	
[a]Winnes et al. (25% load)	MDO	0.5			0.0068 ± 0.0016	
	HFO	0.1			0.71 ± 0.37	
[a]Winnes et al. (10% load)	MDO	0.5			0.018 ± 0.0034	
	HFO	0.1			0.45 ± 0.13	

[a]Run without thermal denuder (TD).

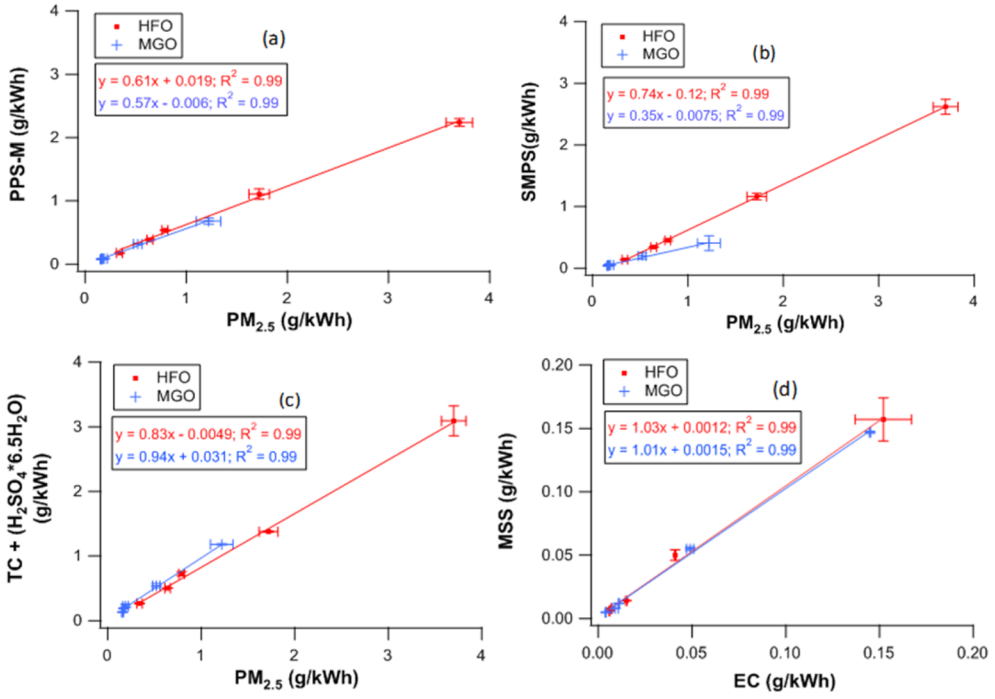

Figure 2. PM Correlations (a) PPS-M sensor versus $PM_{2.5}$ (b) SMPS versus $PM_{2.5}$ (c) TC and hydrated sulfate versus $PM_{2.5}$ (d) MSS versus EC.

observed in NO_x emissions between MGO and HFO. MGO emissions were generally seen to exceed LSHFO for all loads (except 75%) resulting in a ∼5% statistically significant increase in the weighted average (MGO: 10.7 ± 0.03 g/kWh, HFO: 10.2 ± 0.03 g/kWh). These differences can be partially accounted for by the fuel density and viscosity, as fuel injection is a volumetric process. In addition, MGO has a slightly higher density (850.9 kg/m^3) than LSHFO (845.2 kg/m^3); higher density fuels (compared to lower density fuels) have more mass injection per unit volume resulting in higher combustion temperatures and higher thermal NO_x emissions [24−26].

The CO emissions were low as expected for diesel engines. Celo et al.[23] found CO emissions to be 1.3 ± 0.02 g/kWh for IFO60 and 1.2 ± 0.02 g/kWh for MDO in comparison to 1.1 ±

DOI: 10.1021/acs.est.6b02577
Environ. Sci. Technol. 2017, 51, 1868−1875

0.08 g/kWh and 0.9 ± 0.06 g/kWh for MGO and HFO respectively. Statistically higher CO emissions with HFO (compared with MGO) were noted at all loads except at the 100% load. This can be attributed to increased combustion efficiency at higher temperatures caused by fuel density and improved atomization with lower viscosity fuels. The CO_2 emission factors are the lowest for both fuels at the 50% load point where these vessels spend most of their time.

PM Mass Emission Factors. The modal and weighted PM emission factors measured by off-line gravimetric analysis and real-time PM measured by the PPS-M sensor are summarized in Table 4. The highest emission factors were observed at the 10% load point for LSHFO (3.7 ± 0.13 g/kWh) and MGO (1.2 ± 0.12 g/kWh), which decreased with increasing load. PM emissions (g/kWh) for main engine, medium speed OGVs from previous studies are compared against the current in Table 5. $PM_{2.5}$ emissions (0.20 ± 0.02 g/kWh) for MGO were within what was found for Lloyd's services data,[21] U.S. EPA[10] and CARB.[11] (0.17−0.38 g/kWh) For HFO, PM emissions were significantly lower (0.62 ± 0.008 g/kWh) compared to Lloyd's services data,[21] US EPA[10] and CARB[11] (1.3−1.5 g/kWh,), which may be attributed to the lower sulfur content with HFO in the current study.

Weighted $PM_{2.5}$ mass emissions (Table 4) are approximately a factor of 3, lower for MGO (0.20 ± 0.02 g/kWh) than HFO (0.62 ± 0.008 g/kWh). Differences may be partially attributed to the higher sulfur content, density, viscosity and micro carbon residue (MCR) of the fuel. Higher fuel sulfur content (LSHFO-0.009% m/m; MGO-0.005% m/m) will result in more hydrated sulfate contributing to the total fraction of PM while higher density fuels will increase the combustion temperature resulting in an increased thermal combustion efficiency and more oxidized PM. Fuels with higher viscosity are inherently more difficult to atomize into the piston leading to larger fuel droplets and less complete combustion which results in more PM and CO.[27,28] In addition, fuels with higher MCR (amount of residual carbon deposits formed during high internal combustion temperatures.) will form more PM than lower MCR fuels.[29] It is worthy to note that results may vary with the type of engine tested. For example, it is expected that PM will be less for a slow speed engine (compared to medium or high speed engines) due to increased residence time in the combustion chamber and higher injection pressures.

Measurement Comparison. Linear regressions in Figure 2 (a) between the PPS-M sensor and $PM_{2.5}$ measured gravimetrically showed good agreement with R^2 > 0.99 for both fuels. PPS-M sensor data was corrected with a custom calibration using size distribution measured from the SMPS (current study) as default calibration is based on size distributions with an average size of 50 nm.[30] The weighted emission factors show that real-time PM mass measured by the PPS-M sensor is approximately 39% lower than $PM_{2.5}$ Teflon mass for HFO and 57% lower with MGO. Previous studies[31] have shown the PPS-M sensor to exhibit lower PM mass compared to filter based methods. These differences may be attributed to differences in measurement methods. PM filter collection followed ISO-8178 sampling protocol where the diluted sample stream is maintained at a temperature of <52 °C before the filters. Species collected on these filters include solid and semivolatiles. The PPS-M Sensor measures PM at 200 °C while only measuring the solid and some of the volatile species. At these higher temperatures, the PPS-M sensor will not measure the same volatile species collected on the Teflon filters. Amanatidis et al.[30,31] stated from Giechaskiel et al. that heating the PPS-M sensor to 200 °C only partially removes the semivolatile and volatile species. It was concluded that the PPS-M sensor should lie between the AVL MSS and the PM measured gravimetrically.

Figure 2 (b) shows the linear regressions of the PM mass measured from the SMPS versus the $PM_{2.5}$ gravimetric mass. Both methods show good agreement as a function of fuel type with R^2 > 0.99. For the weighted emission factors, PM mass measured by the SMPS is approximately 46% lower than gravimetric $PM_{2.5}$ for LSHFO and 74% lower with MGO. This can be attributed to evaporation due to the high dilution ratios with the SMPS. The sample was diluted at approximately 72:1 before entering the SMPS. The ratio of PM mass calculated from the SMPS and measured gravimetrically for both fuels was compared (Figure 3). This ratio known as the "density correction factor" is the density needed for the SMPS PM mass to equate to the gravimetric PM mass. As the peak mass diameter from the SMPS decreases from HFO to MGO, the density correction factor increases. At smaller diameters (MGO), more evaporation occurs at these high dilution ratios.

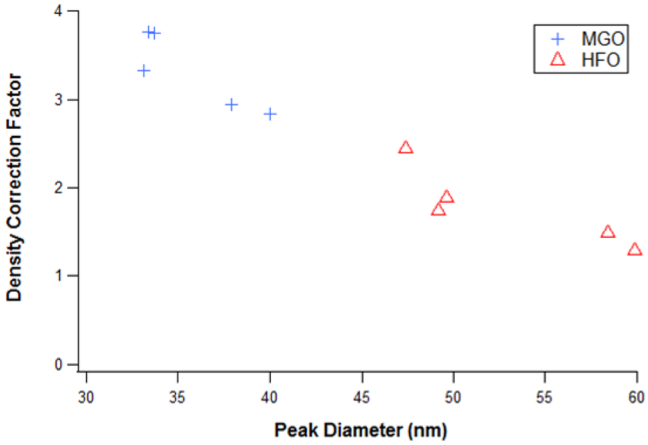

Figure 3. Density correction factor for HFO and MGO.

Previous studies[32,33] have shown that dilution ratio can significantly influence PM mass measurements. Ristimaki et al.[33] looked at the effects of dilution ratio on PM mass for a light fuel oil (LFO) and a HFO. They determined that at a dilution ratio above 40:1, PM measurements approached results of EPA Method 17 commonly used for stationary source measurements while PM mass was sensitive to changes in lower dilution ratios. At high dilution ratios, less condensable species are available for particle growth and formation due to evaporation and only the solid particles remain. This was similarly observed with the SMPS mass (Figure 2 (d)) which showed lower mass than the $PM_{2.5}$ filter measurements. This can be attributed to the high dilution ratios used with the SMPS compared to the $PM_{2.5}$ gravimetric filter samples.

PM Constituents. The modal and weighted emission factors for PM constituents: EC, OC, hydrated sulfate and real-time black carbon measured by the AVL MSS are summarized in Table 4. Overall, EC/OC ratios were very low ranging from 0.02 to 0.05 for HFO and from 0.03 to 0.14 for MGO, which was consistent with those measured in past studies with similar fuels.[9−11] The sum of EC, organic matter (OM) and hydrated sulfate can be compared to the total $PM_{2.5}$ measured gravimetrically on Teflo filters. The organic mass was estimated

DOI: 10.1021/acs.est.6b02577
Environ. Sci. Technol. 2017, 51, 1868−1875

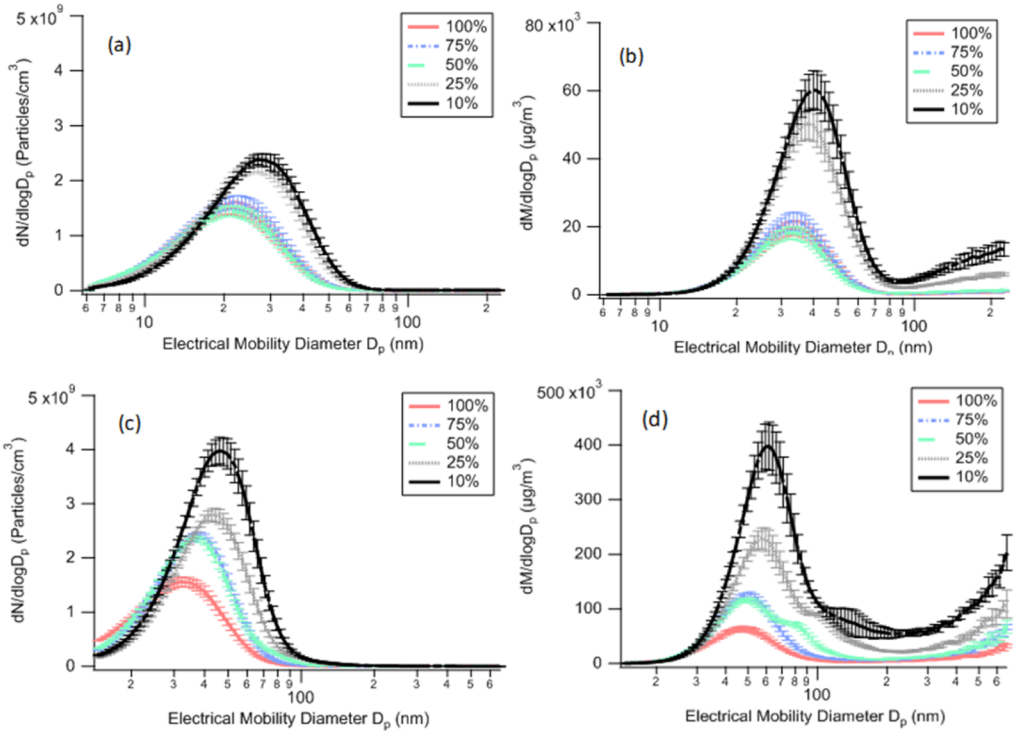

Figure 4. Particle number (a-MGO, c-HFO) and particle mass (b-MGO, d-HFO) concentrations.

by multiplying the OC by a factor of 1.2[34] to account for the oxygen and hydrogen bound to the carbon. This comparison is possible as there is little ash and metals in both fuels, limiting their overall contribution to noncarbon $PM_{2.5}$. Linear regressions (Figure 2 (c)) for both fuels show good agreement (slope = 0.83^{HFO} and slope = 0.92^{MGO}) resulting in good correlations $R^2 > 0.99$.

The correlation between EC collected on quartz filters and analyzed by the NIOSH method and soot measured in real-time by the photoacoustic method AVL MSS are shown in Figure 2 (d). For both HFO and MGO fuels, the resulting linear regressions show good agreement (slope = 1.01^{HFO} and slope = 1.03^{MGO}) with excellent R^2 values > 0.99. Kamboures et al.[35] measured an R^2 of 0.86 for the AVL MSS versus EC determined by the IMPROVE_A method, while Khan et al.[36] measured an R^2 of 0.88 for PM measured by the AVL MSS.

Particle Size Distributions and Particle Number Emission Factors. Particle size distributions (Figure 4) measured by the SMPS for HFO show peak number concentrations at diameters ranging from 30 to 50 nm, compared to 20−30 nm with MGO. Error bars denote the standard deviation from the average of the triplicate load point repeats. At each repeat, the SMPS produced four scans. Previous research conducted by Kasper et al.,[37] showed size distributions for MGO from approximately 40 nm at 100% load to 25 nm at 10% load. They found that at 1% load HFO showed larger mean particle diameters than MGO, whereas at 100% load MGO showed larger mean particle diameters than HFO. Lyyränen et al.[38] found peak number concentrations for HFO at approximately 40−45 nm independent of the load. Figure 4 shows the particle number and particle mass concentrations corrected for dilution ratio as a function of load and fuel type. For LSHFO, the 10% and 25% load points showed the largest peak number and mass concentrations followed by the 50−100% load points. For MGO, both 10% and 25% modes show similar concentrations at 30 nm compared to similar concentrations at 20 nm for the 50−100% load points. The increase in PM mass concentrations with decreasing load points for MGO and LSHFO in Figure 4 (b, d) are consistent with the PM mass results in Table 4. For MGO, peak mass concentrations ranged from 41 and 39 nm with 10% and 25% load points compared to 33 nm with the 50%, 75%, and 100% load points. As the mass is proportional to the D_p^3, the 10% and 25% load points have the highest PM mass followed by the 50−100% load points, agreeing well with the $PM_{2.5}$ gravimetric mass in Table 4. For LSHFO, the peak mass diameters occur at 62 and 57 nm for 10% and 25% load points followed by 50 nm for the 50% and 75% load points and 46 nm with the 100% load point. Similar to MGO, these trends follow the gravimetric $PM_{2.5}$ in Table 4.

Total particle number emissions for the SMPS and PPS-M sensor are shown in Figure 5. The total particle number from the SMPS was determined by integrating the number concentration from the size distributions. Particle size distributions measured by Winnes et al.[39] with HFO shows higher peak number concentrations at $\sim 1 \times 10^{11}$ particles/cm^3 for the 10% and 25% loads and $\sim 1 \times 10^{9}$ particles/cm^3 for the 35% load compared to the current study. Compared to Winnes et al.,[39] PN measured with the SMPS for HFO was almost an order of magnitude lower (at 25% load without a thermal denuder) and ~40% lower with the PPS-M sensor (at 25% load with a thermal denuder). Differences may be attributed to the higher aromatic content, viscosity, PAHs, sulfur and trace metals in the HGO fuel used in Winnes et al.[39]

Overall, the particle number for the PPS-M sensor compared to the integrated SMPS number is 28% higher with LSHFO and 17% higher with MGO. Differences in particle number between the PPS-M sensor and the SMPS are statistically significant for both fuels (except LSHFO at 10% load). As mentioned earlier in the experimental methods, the SMPS

DOI: 10.1021/acs.est.6b02577
Environ. Sci. Technol. 2017, 51, 1868−1875

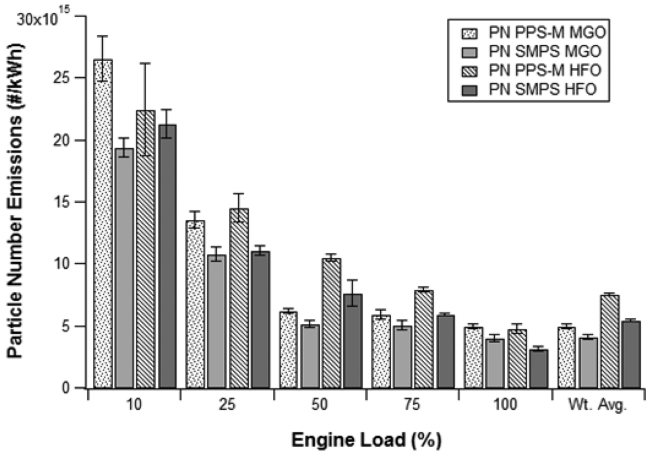

Figure 5. Particle number emissions for HFO and MGO fuels.

measured from a two-stage dilution system consisting of a partial flow venturi diluter as the first stage of dilution and an ejector diluter as the second stage of dilution (72:1 dilution). The PPS-M sensor was measured directly from the partial flow venturi diluter for only one stage of dilution (12:1 dilution). Khalek et al.[40] showed that diesel particulate in the nanoparticle (<50 nm) size range is very sensitive to changes in dilution ratio. With high OC/EC ratios observed in this study, gas to particle conversions will be the dominant mode of growth. Higher dilution ratios will suppress particle growth and therefore less species will be available for heterogeneous nucleation.[41] Similar to this study, previous studies[30,42] with the PPS-M sensor have shown higher PN emissions compared to a TSI model 3010 D CPC and a TSI model 3776 CPC. Differences in measurements may be attributed to the measurement methodology and sampling location. The PPS-M sensor used a heated line (200 °C) to sample PM, whereas the body of the sensor was maintained at 250 °C to avoid thermophoretic losses and condensation. This is compared to the SMPS, which is a nonheated instrument measured. Therefore, both instruments are measuring different particle distributions at their sample inlets. To correct for these differences, the PPS-M sensor was calibrated based on size distributions measured with the SMPS as a function of engine load and fuel type. Corrections were made with the geometric means obtained from the SMPS and applied as multipliers to the measured PPS-M sensor concentrations.

In addition, higher PN emissions with the PPS-M sensor can be partially attributed to its low-cut point of a few nm compared to the SMPS. For the SMPS, a wider size range was used for LSHFO (compared to MGO) as larger particle sizes were observed. The lower size limit used for LSHFO measurements was 15 nm compared to 6 nm with MGO. As the cut points for both instruments are more similar for MGO than LSHFO, this may be partially why there is only a 17% difference with MGO compared to the 28% difference with LSHFO between the PPS-M sensor and SMPS.

Implications. Ocean Going Vessels (OGVs) contribution to worldwide emissions inventories has increased in the past decade due to emissions reductions in the transportation sector initiated by improvements in engine technology and aftertreatment devices. Furthermore, a large fraction of emissions from OGVs occurs within close proximity to land or nearby port communities, which has significant negative implications for local air pollution and adverse health effects.

NOx and CO emissions measured in this study were below US EPA[15] and CARB[16] values, but larger than those measured by Cielo et al.[23] PM emissions were similar to MGO and slightly higher with LSHFO compared to Cielo et al.[23] Due to the complex nature of PM growth and formation (primarily from condensables), measurement location and methodology will strongly influence PM results. In this study, the total PM measured by the PPS-M sensor and SMPS were well below the $PM_{2.5}$ gravimetric measurements. This can be attributed to differences in measurement methodology, sampling parameters and sampling location. Real-time PM measurements should be used to supplement regulatory PM filter methods and characterize emissions trends in real-time.

In regards to policy considerations, the LSHFO is a viable alternative to conventional HFO with ∼25% reduction in NO_x emissions and ∼50% reduction in PM mass emissions. Results suggest that PN emissions are lower than those of higher sulfur HFO fuels. Refs 24, 25, 26.

AUTHOR INFORMATION

Corresponding Author

*E-mail: dcocker@engr.ucr.edu.

ORCID

Nicholas R. Gysel: 0000-0001-6433-7444

Notes

The authors declare no competing financial interest.

ACKNOWLEDGMENTS

We express our gratitude towards the California Air Resources Board (CARB) for their financial support, the suppliers of the novel fuel and the crude carrier for the generous access to their vessel. We specifically thank the CE-CERT analytical Emissions Laboratory at CE-CERT and Mr. Kurt Bumiller for his help with the test preparations.

REFERENCES

(1) Merk, Olaf. Shipping Emissions in Ports. *International Transport Forum* **2014**, DOI: 10.1787/5jrw1ktc83r1-en.

(2) Corbett, J. J.; Winebrake, J. J.; Green, E. H.; Kasibhatla, P.; Eyring, V.; Lauer, A. Mortality from Ship Emissions: A Global Assessment. *Environ. Sci. Technol.* **2007**, *41* (24), 8512−8518.

(3) United Nations Conference on Trade and Development (UNCTAD). *Review of Maritime Transport*, 2014.

(4) Corbett, J. J.; Fischbeck, P. S. Emissions from Waterborne Commerce Vessels in United States Continental and Inland Waterways. *Environ. Sci. Technol.* **2000**, *34* (15), 3254−3260.

(5) Pope, C. A., III; Dockery, D. W. Health effects of fine particulate air pollution: Lines that connect. *J. Air Waste Manage. Assoc.* **2006**, *56*, 709−742.

(6) Pope, C. A., III; Ezzati, M.; Dockery, D. W. Fine-particulate air pollution and life expectancy in the United States. *N. Engl. J. Med.* **2009**, *360* (4), 376−386.

(7) International Maritime Organization Sub-Committee on Bulk Liquids and Gases. Review of MARPOL annex VI and the NO_x technical note, development of standards for NO_x, PM and SO_x. ww.arb.ca.gov/research/seca/imo07b.pdf.

(8) International Maritime Organization (IMO). *Annex VI of MARPOL 73/78, Regulations for the Prevention of Air Pollution from Ships and NO_x Technical Code*; Det Norske Veritas (DNV): Høvik, Norway, 2005.

(9) Agrawal, H.; et al. In-use gaseous and particulate matter emissions from a modern ocean going container vessel. *Atmos. Environ.* **2008**, *42* (21), 5504−5510.

(10) Agrawal, H.; et al. Emissions from main propulsion engine on container ship at sea. *J. Geophys. Res.* **2010**, *115*, 115.

DOI: 10.1021/acs.est.6b02577
Environ. Sci. Technol. 2017, 51, 1868−1875

(11) Agrawal, H.; et al. Emission measurements from a crude oil tanker at sea. *Environ. Sci. Technol.* **2008**, *42* (19), 7098−7103.
(12) Khan, M. K.; et al. Benefits if Two Mitigation Strategies for Container Vessels: Cleaner Engines and Cleaner Fuels. *Environ. Sci. Technol.* **2012**, *46*, 5049−5056.
(13) Cooper, D. A. Exhaust emissions from ships at berth. *Atmos. Environ.* **2003**, *37*, 3817−3830.
(14) Entec UK Limited. *Quantification of Emissions from Ships associated with Ship Movements between Ports in the European Community*. 2002.
(15) U.S. Environmental Protection Agency. *Current Methodologies and Best Practices in Preparing Port Emission Inventories: Final Report*; April, 2009; http://epa.gov/cleandiesel/documents/ports-emission-inv-april09.pdf.
(16) California Air Resources Board. Emissions Estimation Methodology for Ocean-Going Vessels. 2011. http://www.arb.ca.gov/regact/2011/ogv11/ogv11appd.pdf.
(17) International Organization for Standardization (ISO). ISO 8178−2, Reciprocating Internal Combustion Engines: Exhaust Emission Measurement. Part-2: Measurement of Gaseous Particulate Exhaust Emissions at Site; ISO: Geneva, Switzerland, 1996.
(18) Protection of the Environment. Title 40. Sections 86 and 89. U.S. Code of Federal Regulations.
(19) NIOSH, 1996. NIOSH Manual of Analytical Methods. National Institute of Occupational Safety and Health, Cincinnati, OH.
(20) Lehtimäki, M. Modified Aerosol Detector. In *Aerosols in Mining and Industrial Work Environment*; Marple, V.A., Liu, B.Y.H. Eds.; Ann Arbor Science Publishers: Ann Arbor, MI, 1983; Vol. 3, pp 1135−1143.
(21) Lloyd's Register. *Lloyd's Register Engineering Services*, 1990a, 1990b, 1993a, 1993b & 1995.
(22) International Organization for Standardization (ISO). *Reciprocating Internal Combustion Engine-Exhaust Emission Measurement-Part 4: Test Cycles for Different Engine Applications*, ISO 8178-4, 1996.
(23) Celo, V.; Dabek-Zlotorzynska, E.; McCurdy, M. Chemical Characterization of Exhaust Emissions from Selected Canadian Marine Vessels: The Case of Trace Metals and Lanthanoids. *Environ. Sci. Technol.* **2015**, *49* (8), 5220−5226.
(24) Ban-Weiss, G. A.; Chen, J.; Buchholz, B. A.; Dibble, R. W. A numerical investigation into the anomalous light NOx increase when burning biodiesel; a new(old) theory. *Fuel Process. Technol.* **2007**, *88*, 659−67.
(25) Alptekin, E.; Canakci, M. Determination of the density and the viscosities of biodiesel−diesel fuel blends. *Renewable Energy* **2008**, *33*, 2623−30.
(26) McCormick, R. L.; Graboski, M. S.; Alleman, T. L.; Herring, A. M.; Tyson, K. S. Impact of biodiesel source material and chemical structure on emissions of criteria pollutants from a heavy-duty engine. *Environ. Sci. Technol.* **2001**, *35*, 1742−7.
(27) Northrop, W. F.; P. V., Madathil; Bohac, S. V.; Assanis, D. N. Condensational growth of particulate matter from partially premixed low temperature combustion of biodiesel in a compression ignition engine. *Aerosol Sci. Technol.*, vol. *45*, no. 1, pp 26−36, **2011**.10.1080/02786826.2010.517579
(28) Deqing, M.; Junnan, Q.; Ping, S.; Yan, M.; Shuang, Z.; Yongjun, C. Study on the combustion process and emissions of a turbocharged diesel engine with EGR. *J. Combust.*, vol. **2012**, Article ID 932724, 9 pages, *2012*2012.10.1155/2012/932724
(29) Totten, G. E.; Westbrook, S.; Shah, R. J. Fuels and Lubricants Handbook-Technology, Properties, Performance, and Testing. *ASTM International* **2013**, 07−15.
(30) Giechaskiel, B.; Drossinos, Y. (2010). Theoretical Investigation of Volatile Removal Efficiency of Particle Number Measurement Systems. *SAE Technical Paper* **2010**, *3*, 01−1304.
(31) Amanatidis, S., Ntziachristos, L., Samaras, Z., Janka, K. et al., "Applicability of the Pegasor Particle Sensor to Measure Particle Number, Mass and PM Emissions," *SAE Tech. Pap. Ser.* 2013−24−0167, **2013**, doi:10.4271/2013-24-0167.
(32) Moldanová, J.; Fridell, E.; Popovicheva, O.; Demirdjian, B.; Tishkova, V.; Faccinetto, A.; Focsa, C. Characterisation of particulate matter and gaseous emissions from a large ship diesel engine. *Atmos. Environ.* **2009**, *43*, 2632−2641.
(33) Ristimaki, J.; Hellem, G.; Lappi, M. Chemical and physical characterization of exhaust particulate matter from a marine medium speed diesel engine. *CIMAC Congress, Bergen, Norway*, 2010
(34) Shah, S. D.; Cocker, D. R., III; Miller, J. W.; Norbeck, J. M. Emission rates of particulate matter and elemental and organic carbon from in-use diesel engines. *Environ. Sci. Technol.* **2004**, *38*, 2544−2550.
(35) Kamboures, M. A.; Shishan, H.; You, Y.; Sandoval, J.; Rieger, P.; Hugan, S-M. H; Zhang, S.; Dzhema, I.; Huo, D.; Ayala, A.; Oliver Change, M. C. Black carbon emissions in gasoline vehicle exhaust: A measurement and instrument comparison. *J. Air Waste Manage. Assoc.* **2013**, *63*, 886−901.
(36) Khan, M. Y.; Johnson, K. C.; Durbin, T. D.; Jung, H.; Cocker, D. R., III; Bishnu, J. Giannelli, Characterization of PM-PEMS for in-use measurements conducted during validation testing for the PM-PEMS measurement allowance program. *Atmos. Environ.* **2012**, *55*, 311−318.
(37) Kasper, A.; et al. Particulate emissions from a low-speed marine diesel engine. *Aerosol Sci. Technol.* **2007**, *41* (1), 24−32.
(38) Lyyŕanen, J.; Jokiniemi, J.; Kauppinen, E. I.; Joutsensaari, J. Aerosol Characterisation in Medium-Speed Diesel Engines Operating with Heavy Fuel Oils. *J. Aerosol Sci.* **1999**, *30*, 771−784.
(39) Winnes, H., Fridell, E., Hallquist, A., Anderson, M., Salo, K. *Characterization of Particle Emissions from Marine Engines with Emphasis on Nanoparticles*, IVL Report B 2198; Swedish Research Institute, June 2014.
(40) Khalek, I. A.; Kittelson, D.; Brear, F. The Influence of Dilution Conditions in Diesel Exhaust Particle Size Distribution Measurements. *SAE Tech. Pap. Ser.* **1999**, 01−1142.
(41) Kittelson, D. B. Engines and nanoparticles: a review. *J. Aerosol Sci.* **1998**, *29* (5−6), 575−588.
(42) Ntziachristos, L.; Amanatidis, S.; Samaras, Z. Application of the Pegasor Particle Sensor for the Measurement of Mass and Particle Number Emissions. *SAE Technical Paper* **2013**, 01−1561 2013.

DOI: 10.1021/acs.est.6b02577
Environ. Sci. Technol. 2017, 51, 1868−1875